Array Pattern Distortion and Remedies in Space–Time Adaptive Processing for Airborne Radar

Renbiao Wu, *Member, IEEE*, and Zheng Bao, *Senior Member, IEEE*

***Abstract*—Space–time adaptive processing (STAP) for airborne early warning radar has been a very active area of research since the late 1980's. An airborne rectangular planar array antenna is usually configured into subarrays and then partial adaptive processing is applied to the outputs of these subarrays. In practice, three kinds of errors are often encountered, i.e., the array gain and phase errors existing in each element, the channel gain and phase errors, and the clutter covariance matrix estimation errors due to insufficient secondary data samples. These errors not only degrade the clutter suppression performance, but also cause the adapted array patterns to suffer much distortion (high sidelobes and distorted mainbeams), which may result in the rise of false-alarm probability and make the adaptive monopulse tracking and sidelobe blankering more difficult. In this paper, the causes of the above three kinds of errors to array pattern distortion are discussed and a novel quadratic soft constraint factored approach is proposed to precisely control the peak sidelobe level of adapted patterns. The soft constraint factor can be determined explicitly according to the peak sidelobe level desired and the known or desired tolerant error standard deviations. Numerical results obtained by using high-fidelity simulated airborne radar clutter data are provided to illustrate the performance of the proposed approach. Although the method is presented for STAP, it can be directly applied to the conventional adaptive beamforming for rectangular planar arrays used to suppress jammers.**

***Index Terms*—Adaptive arrays, airborne radar.**

I. Introduction

AIRBORNE early warning radar is very useful for the detection of small radar cross-section (RCS) targets in severe clutter. Unlike ground-based radar in which nearly all the clutter return is received at or near zero Doppler due to the platform motion, the clutter return in an airborne radar has widely spread Doppler frequencies. A conventional airborne moving target indicator (AMTI) is ineffective in canceling airborne radar clutter because it uses temporal degrees of freedom only and only the mainlobe clutter can be removed in this way. Much better clutter suppression performance can be obtained by fully exploiting the distribution characteristics of the airborne clutter spectrum in the spatial-Doppler (or spatial-temporal) domain and adaptively forming two-dimensional nulls matched to the clutter spectrum distribution. This is the basic idea behind space–time adaptive processing (STAP) which was first proposed in [1] in 1973. With the availability of ever-improving phased-array antenna and advanced digital signal processing technology, there has been a renewed interest in STAP since the late 1980's. So far, several STAP algorithms have been developed in [2]–[5] and a very good review about the state-of-the-art advances of STAP technology can be found in [6].

It is commonly believed that STAP has the potential to improve the performance of an airborne early warning radar without the costly antenna refinements normally needed to reduce array sidelobes and correspondingly, clutter. Hence, a practical STAP algorithm should be robust against various kinds of mismatch errors. Although theoretic performance prediction of many existing STAP algorithms is excellent, their practical performance is not so encouraging. Many algorithms suffer significant performance degradation when there exist mismatch errors. How to improve the robustness of STAP algorithms is a very important issue and has become the current research focus.

Usually, an airborne radar uses a rectangular planar phased-array antenna. To reduce the cost of both the receivers and the signal processors, the planar array is usually configured into subarrays by using analog beamforming to the columns of the array and then (adaptive) digital beamforming is applied to the outputs of these subarrays. For airborne sidelooking radar working at high-pulse repetition frequency (HPRF) mode, the range is highly ambiguous and the clutter return of each range bin is the superposition of many clutter echoes coming from different ranges with different depression angles. In this case, we have found that the array errors not only have significant effects on the clutter suppression performance [5], [7], but also cause the adapted array patterns suffer much distortion (high sidelobes and distorted mainlobes), which may result in the rise of false-alarm probability and make the adaptive monopulse tracking and sidelobe blankering more difficult.

For conventional adaptive arrays used to suppress jammers, the pattern distortion caused by interference covariance matrix estimation errors due to insufficient secondary data samples has received significant attention in the published literatures [8]–[10]. Diagonal loading (or noise injection) [9] is a simple and effective way to remedy the pattern distortion caused by the covariance matrix estimation errors. However, the diagonal loading value is usually chosen by rule of thumb. In [11],

Manuscript received November 21, 1995; revised May 30, 1996. This work was supported by the Chinese National Science Foundation under Grant 69 572 033.

R. Wu is with the Department of Electronic Engineering, Civil Aviation Institute of China, Tianjin, 300300, China.

Z. Bao is with the State Key Laboratory for Radar Signal Processing, Xidian University, Xi'an, 710071, China.

Publisher Item Identifier S 0018-926X(98)05772-X.

0018–926X/98$10.00 © 1998 IEEE

we have proposed a method that can be used to precisely control the peak sidelobe level in conventional full adaptive linear arrays when both array and covariance matrix estimation errors exist. In this paper, the differences of the effects of array, channel, and estimation errors on the adaptive array patterns in STAP are discussed and a method is proposed that can remedy this distortion and precisely control the peak sidelobes to the desired level according to the known or desired tolerant error standard deviations. The proposed method can also be directly applied to the conventional partial adaptive planar arrays used to suppress jammers.

The remainder of this paper is organized as follows. Section II discusses the effects of different errors on the array patterns and gives an upper limit on the practical peak sidelobes of adaptive patterns. The proposed adaptive pattern control method is given in Section III. Some numerical examples are provided in Section IV to illustrate the performance of the proposed method. Finally, Section V contains our conclusion.

II. Effect of Errors on Adapted Patterns

Suppose the airborne phased-array antenna is a rectangular planar array composed of M (rows) $\times$ N (columns) omnidirectional elements. We assume that each column of the array is synthesized by using a separate analog beamformer and STAP is applied to the outputs of the equivalent horizontal linear array with N "elements" (column subarrays).

For airborne sidelooking radar whose antenna normal is perpendicular to the platform flight direction, parallel to the factored approach referenced by [6], we independently proposed a STAP algorithm notated as TF$SAP (temporal filtering then spatial adaptive processing) in [5]. TF$SAP is a factored approach that encompasses multichannel AMTI and Doppler filtering with ultralow sidelobes followed by adaptive beamforming for each Doppler bin and the block diagram can be found in [5] and [7]. Compared to the joint-domain adaptive processing approaches, TF$SAP performs well for those Doppler bins well separated from the mainlobe clutter region, but suffers some performance degradation in the mainlobe clutter region. TF$SAP is a good candidate STAP scheme for airborne radar working in the HPRF mode since in this case, the mainlobe clutter region is limited to only a few Doppler bins and some of them must be discarded due to the necessary ground traffic filtering over slow moving vehicles. In addition, it has very good compatibility with other radar functions, such as space-time adaptive monopulse tracking and space-time adaptive sidelobe blankering [12]. TF$SAP significantly outperforms the joint-domain adaptive processing algorithms in the implementation cost and is ready to be implemented using currently available digital signal processing (DSP) chips [12].

In practical airborne array antennas, there are many kinds of mismatch error sources, such as mutual coupling and channel frequency response mismatch errors. Although it is commonly believed that STAP can relieve the requirement for costly antenna refinements, careful monitoring and calibration of these errors are still necessary for STAP so as to achieve greater performance improvement over the conventional nonadaptive processing approach. Even after calibration, small residue errors still exist. Like [13], we model the residue errors after calibration as amplitude and phase errors in the array elements (abbreviated as array errors) and in the receiver channels (abbreviated as channel errors).[1] Assume there are K Doppler bins and the adaptive weight vector applied to the kth Doppler bin $(1 \le k \le K)$ is denoted by $\mathbf{W}_k \triangleq [W_{k1}\ W_{k2}\ \cdots\ W_{kN}]^T$ where $(\cdot)^T$ denotes the transpose. Then the adaptive array pattern for the kth Doppler bin is given by

$$H_k(\psi,\varphi) = \sum_{n=1}^{N} W_{kn}^* H_{\mathrm{sb}n}(\varphi)\left(1+\delta_n^c\right)\exp\left(j\phi_n^c\right) \times \exp\left(j\frac{2\pi d_x}{\lambda} n\cos\psi\right) \tag{1}$$

where

$$H_{\mathrm{sb}n}(\varphi) = \sum_{m=1}^{M} I_m\left(1+\delta_{mn}^a\right)\exp\left(j\phi_{mn}^a\right) \times \exp\left[j\frac{2\pi d_y}{\lambda} m(\sin\varphi - \sin\varphi_0)\right] \tag{2}$$

ψ: the bearing cone angle; φ: the depression angle; (ψ_0,φ_0): the beam pointing angle; $(\cdot)^*$: the complex conjugate; d_x and d_y: the horizontal and vertical element spacings, respectively; λ: the radar wavelength; δ_{mn}^a and ϕ_{mn}^a: the amplitude and phase errors in the element located at the mth row and the nth column, respectively; δ_n^c and ϕ_n^c: the amplitude and phase errors in the nth receiver channel, respectively; $I_m's (1 \le m \le M)$: the weights used by the analog beamformer to each column of the array; and $H_{\mathrm{sb}n}(\varphi)$: the nth column-subarray pattern in the presence of array errors. δ_{mn}^a, ϕ_{mn}^a, δ_n^c, and ϕ_n^c are modeled as zero-mean independent random variables with standard deviations σ_a^a, σ_ϕ^a, σ_a^c, and σ_ϕ^c, respectively.

When there is no interference and infinite secondary data samples are available, the adaptive weight vector $\mathbf{W}_k$ $(1 \le k \le K)$ degenerates into the quiescent weight vector $\mathbf{S}_q$. Usually, the quiescent weight vector $\mathbf{S}_q$ is designed to steer the beam to a given look direction and yield low sidelobes to suppress the pulse interference and strong unwanted target signals entering into the sidelobe regions. Define $\mathbf{S}_q$ (3), shown at the bottom of the page, where $A_n's$ $(1 \le n \le N)$ are the quiescent weight settings to provide low sidelobe patterns.

We would like first to analyze the pattern distortion caused by array and channel errors in a nonadaptive rectangular planar array and this is helpful for us to determine an upper limit on the attainable peak sidelobe level of adaptive patterns. Let us

[1] In [13], array and channel errors are defined as uncorrelated and correlated array errors, respectively.

$$\mathbf{S}_q = \left[A_1 e^{j\frac{2\pi d_x}{\lambda}\cos\psi_0} \quad A_2 e^{j\frac{2\pi d_x}{\lambda}2\cos\psi_0} \quad \cdots \quad A_N e^{j\frac{2\pi d_x}{\lambda}N\cos\psi_0}\right]^T \tag{3}$$

set the adaptive weight vector $\mathbf{W}_k = \mathbf{S}_q$ in (1) and denote the array pattern so obtained by $H_q(\psi, \varphi)$. If the number of array elements is not so small and the random array and channel errors are not very large and independent with each other, then according to Lindenberg and Levy's central limit theorem, under some general conditions the distribution of $H_q(\psi, \varphi)$ is asymptotically normal. The sidelobe level of the normalized radiation pattern obeys Rician distribution. Without loss of generality and assuming that $\sum_{n=1}^{N} A_n = 1.0$ and $\sum_{m=1}^{M} I_m = 1.0$, then it can be deduced (see Appendix A) that in the principal plane corresponding to $\varphi = \varphi_0$ (the worst case), no matter how low the designed peak sidelobe level is, a level for practical peak sidelobes referred to as "PPSL" not to exceed with a confidence probability 99.9% is given by[2]

$$\begin{aligned}\text{PPSL} = 8 + 10\log_{10}\{\|\mathbf{S}_q\|_2^2[(\sigma_a^c)^2 + (\sigma_\phi^c)^2 \\ + \eta[(\sigma_a^a)^2 + (\sigma_\phi^a)^2]]\} \text{ (dB)}\end{aligned} \tag{4}$$

where $\eta = \sum_{m=1}^{M} I_m^2$ and $\|\cdot\|$ denotes the Frobenius norm.

In the presence of array and channel errors, the practical beam pattern is composed of two parts, i.e., the designed pattern and the perturbed component. The perturbed component is random and approximately uniformly distributed in all directions. When the array and channel errors are small, they have little effects on the mainlobes. However, even small errors have significant effects on the sidelobes. For a given designed peak sidelobe level, when the errors become large enough the perturbed component is the dominant contribution to the practical sidelobes. In this case, the practical peak sidelobe level of quiescent patterns is mainly determined by the array and channel error standard deviations and is almost independent of the designed peak sidelobe level, which can be noted from (4). Hence, PPSL is an upper limit for the peak sidelobes of the adaptive array patterns with $\mathbf{S}_q$ as the quiescent weight settings. Furthermore, $\eta[(\sigma_a^a)^2 + (\sigma_\phi^a)^2]$ can be viewed as the equivalent channel error variance due to array errors. Hence, (4) indicates that the pattern distortion caused by the equivalent channel errors (practical channel errors plus the equivalent parts of array errors) cannot be remedied.

In STAP, the pattern distortion comes from two parts, i.e., the perturbation of adaptive weights to the quiescent weight settings and the equivalent channel errors. Since the latter part is not controllable, we must try to reduce the perturbation of adaptive weights to the quiescent weight settings. The array errors and covariance matrix estimation errors contribute much more to this perturbation than the channel errors. The estimation errors will cause the divergence of the noise eigenvalues and result in the pattern distortion. The effect of array errors on STAP is quite different from that on the conventional adaptive arrays. When there are no array errors, all the N column-subarray patterns $H_{\text{sbn}}(\varphi)'s$ $(1 \le n \le N)$ defined in (2) are identical and equal to $\sum_{m=1}^{M} I_m \exp[j\frac{2\pi d_y}{\lambda} m(\sin\varphi - \sin\varphi_0)]$. In this case, the clutter is approximately homogeneous along the range domain. However, in the presence of array errors, the N column-subarray patterns are no longer identical. For HPRF airborne radar, the range is highly ambiguous. The clutter return of each range bin is the sum of many clutter echoes coming from multiple ambiguous ranges with different depression angles. Since the normalized relationships among $H_{\text{sbn}}(\varphi)'s$ $(1 \le n \le N)$ are different from angle to angle, the clutter is no longer homogeneous along the range domain [7]. Like the estimation errors, array errors also cause the noise eigenvalues to diverge and, hence, results in the pattern distortion. This happens even when infinite secondary data samples are available. Nevertheless, the effect of array errors is more severe than that of the estimation errors since array errors increase the dimension size of the clutter subspaces and violate the homogeneous clutter distribution along the range domain. It is usually more difficult to remedy the pattern distortion in STAP than that in the conventional adaptive arrays used to suppress jammers.

[2] In [13], the normalized relationship between errors and sidelobe levels was also discussed. Unfortunately, the results for planar arrays are incorrect.

III. Control of Peak Sidelobe Level in STAP

As pointed out in the previous section, to remedy the pattern distortion caused by adaptive processing we must try to reduce the perturbation of adaptive weights to the quiescent weight settings. Instead of using the hard constraint $\mathbf{W}_k^H \mathbf{S}_q = 1.0$ as used in [5] and [7], where $(\cdot)^H$ denotes the conjugate transpose. Below, we present a factored STAP algorithm with soft constraint that can be formulated as the following optimization problem:

$$\text{minimize} \quad \mathbf{W}_k^H \hat{\mathbf{R}}_k \mathbf{W}_k \tag{5}$$

$$\text{subject to} \quad \frac{\|\mathbf{W}_k - \mathbf{S}_q\|_2^2}{\|\mathbf{S}_q\|_2^2} \le \epsilon_0^2 \tag{6}$$

where $\hat{\mathbf{R}}_k$ denotes the estimated clutter covariance matrix corresponding to the kth Doppler bin and ϵ_0 is a small positive soft constraint factor satisfying $\epsilon_0 < 1$.

It can be proved that by constraining the perturbation of the adaptive weights to the quiescent weight settings using (6), the peak sidelobe level of the adaptive patterns can be controlled to the desired level (to be discussed later on). It can also be shown that the soft constraint plays the role of diagonal loading. Using the Lagrange multiplier method it can be found that the solution to (5) subject to the soft constraint (6) is

$$\mathbf{W}_k = L(\hat{\mathbf{R}}_k + L\mathbf{I})^{-1}\mathbf{S}_q \tag{7}$$

where $\mathbf{I}$ denotes the identity matrix and L is the loading value to be determined, which satisfies the following equation:

$$\|\mathbf{W}_k - \mathbf{S}_q\|_2^2 = \epsilon_0^2 \|\mathbf{S}_q\|_2^2. \tag{8}$$

Take eigenvalue decomposition with $\hat{\mathbf{R}}_k$ then we have

$$\hat{\mathbf{R}}_k = \mathbf{U}\mathbf{\Lambda}\mathbf{U}^H \tag{9}$$

where $\mathbf{U}$ denotes a matrix with the N eigenvectors of $\hat{\mathbf{R}}_k$ as its columns and $\mathbf{\Lambda}$ is a diagonal matrix with the N eigenvalues λ_n $(1 \le n \le N)$ as its diagonal elements. After some simple mathematical manipulations, (8) can be transformed into

$$f(L) \triangleq \sum_{n=1}^{N} \left(\frac{\lambda_n}{L + \lambda_n}\right)^2 |\tilde{S}_{qn}|^2 = \epsilon_0^2 \|\mathbf{S}_q\|_2^2 \tag{10}$$

where $[\tilde{S}_{q1} \;\; \tilde{S}_{q2} \;\; \cdots \;\; \tilde{S}_{qN}]^T \triangleq \mathbf{U}^H \mathbf{S}_q$.

Since $f(L)$ is a monotonically decreasing function with respect to the variable L, the loading value can be calculated using fast algorithms, such as the bisection root-finding method.

The remaining problem is how to determine the value of ϵ_0 according to the peak sidelobe level desired referred to as PSLD. Since PPSL in (4) is an upper limit on the peak sidelobes of both adaptive and nonadaptive array patterns, PSLD must be higher than PPSL. Let's treat the difference between the adaptive and quiescent weight settings as additional channel mismatch errors added to the real array and channel errors. After some similar mathematical manipulations as used in [11], under some mild conditions we can obtain the relationship among the PSLD, the array and channel error standard deviations and the soft constraint factor ϵ_0 as follows (see Appendix for details):

$$\mathrm{PSLD} = 8 + 10\log_{10}\left\{\|\mathbf{S}_q\|_2^2\left[\epsilon_0^2 + \left(\sigma_a^c\right)^2 + \left(\sigma_\phi^c\right)^2 + \eta\left[\left(\sigma_a^a\right)^2 + \left(\sigma_\phi^a\right)^2\right]\right]\right\}(\mathrm{dB}). \tag{11}$$

If the array and channel error standard deviations are known *a priori*, then ϵ_0 can be directly determined from (11) according to the desired peak sidelobe level. Otherwise, we can determine a value of ϵ_0 with desired tolerant capability for array and channel mismatch errors. Equation (11) also indicates that the standard deviations of array and channel errors determine an upper limit on the attainable peak sidelobe level [PPSL defined by (4)] and diagonal loading cannot remedy the pattern distortion caused by the real channel errors and the equivalent parts of the array errors.

Once ϵ_0 is evaluated according to (11), the loading value can be obtained by solving for (10). The amount of computations required to compute the loading value is much greater than that needed to calculate the adaptive weights defined by (7). Solving one loading value for each Doppler bin is too computationally expensive. Fortunately, we have found that apart from a few bins in the vicinity of the mainlobe clutter region, the normalized loading values for all other Doppler bins are almost the same. Herein, the normalized loading value is defined to be the ratio of the loading value to the noise power corresponding to the same Doppler bin. In this case, once one loading value is obtained the loading values for all other Doppler bins can be determined according to this value and the known or estimated noise power (with the modulation effect of the AMTI considered). Hence, the cost of loading value calculation is shared by K Doppler bins. Since for HPRF radar K tends to be very large ($K = 64, 128$, or more larger), the additional cost of calculating loading value is trivial in contrast to that needed by the TF$SAP method.

The calculation of the loading value can be further simplified using parallel algorithms without eigenvalue decomposition. In our STAP scheme, K adaptive weight vectors can be computed independently. This coarse-gridded parallelism can be exploited to implement our algorithm very efficiently using a single-instruction multiple-data (SIMD) parallel processing structure. We can calculate the adaptive weight vectors at some quantitized loading values in parallel according to (7) and then find the best one satisfying (8) as the desired loading value by utilizing the fact that $f(L)$ is a monotonically decreasing function with respect to the loading value L. This scheme makes better use of the parallel processing structure and the adaptive weight calculation code of the signal processor. It has been implemented in an STAP signal processor [12] built with many DSP chips (TMS320C30, A41102, A100).

Since our STAP scheme is basically a factored approach that transforms the space–time adaptive processing into adaptive beamforming for multiple Doppler bins, hence, the above analysis and the beam pattern control method can be directly applied to the conventional adaptive beamforming for rectangular planar arrays used to suppress jammers such as the shipborne surveillance radar used in [14].

IV. Numerical Examples and Discussions

In the State Key Laboratory for Radar Signal Processing, Xidian University, China, a software has been developed to simulate the airborne radar clutter data with high fidelity. The software can simulate video signals with a wide variety of system and environmental mismatch errors taken into account. In this section, we present some numerical results based on these data to illustrate the performance of the proposed method.

In the following examples, we assume: the number of columns $N = 32$; the number of rows $M = 16$; the number of Doppler bins $K = 64$ (not including the two pulses used in AMTI); the radar wavelength $\lambda = 0.2$ m; the pulse repetition frequency $= 5000$ Hz; the array-element spacings $d_x = d_y = 0.1$ m; the platform flight velocity $= 250$ m/s; the platform altitude $= 10$ km; the beam-pointing angle $(\psi_0, \varphi_0) = (90°, 0°)$; $A_n's$ $(1 \le n \le N)$; and $I_m's$ $(1 \le m \le M)$ are Chebyshev weights with -40- and -30-dB peak sidelobes, respectively, and the Doppler filters employ Chebyshev weights with -70-dB peak sidelobes. To simplify the notations, let "E" and "C" denote the array and channel error standard deviations, respectively. For example, $E = 5\%$ means that $\sigma_a^a = \sigma_\phi^a = 5\%$ where $\sigma_\phi^a = 5\%$ means $\sigma_\phi^a = 0.05$ radians. Unless otherwise stated, all the results presented below are for No. 13 Doppler bin.

First, we present an example to illustrate the special effect of array errors on the pattern distortion in STAP. The covariance matrix estimation errors and the channel errors have similar effects on the array pattern distortion for both STAP and the conventional adaptive arrays [11]. (Since the discussion in [11] is based on full adaptive linear array, in that case, the array and channel errors can be treated as one. The array errors in [11] correspond to the channel errors herein.) However, the effect of array errors on STAP is more severe than that on conventional adaptive arrays. Fig. 1(a) compares the clutter eigen spectra in cases with ($E = 5\%$) and without ($E = 0\%$) array errors. It can be noted from Fig. 1(a) that array errors not only cause the noise eigenvalues of the clutter covariance matrix to diverge and result in the pattern distortion, but also greatly increase the dimension size of the clutter subspace. The adaptive pattern in the error-free case is shown in Fig. 1(b). Note that when there are no errors, the adaptive pattern has formed a very deep null in the sidelobe clutter region corresponding to the Doppler

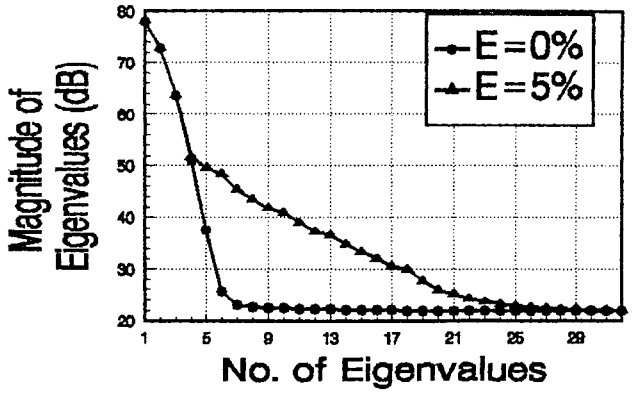

(a)

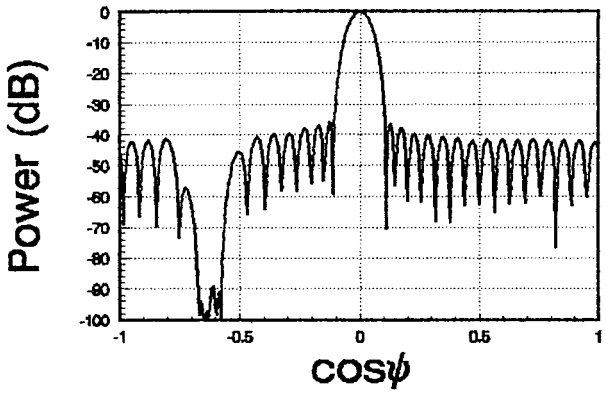

(b)

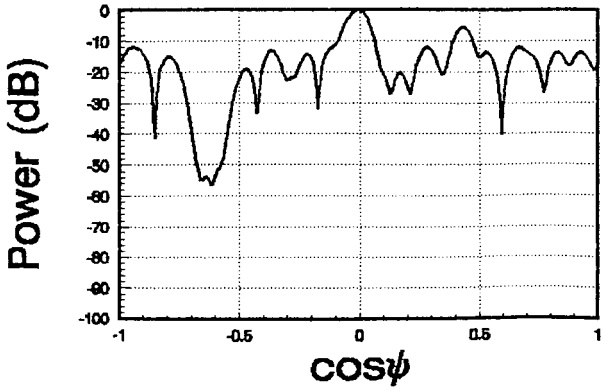

(c)

Fig. 1. Effect of array errors on the adaptive pattern distortion. (a) Comparison of clutter eigenspectra with ($E = 5\%$) and without ($E = 0\%$) array errors. (b) Adaptive pattern in the absence of array errors. (c) Adaptive pattern in the presence of array errors ($E = 5\%$).

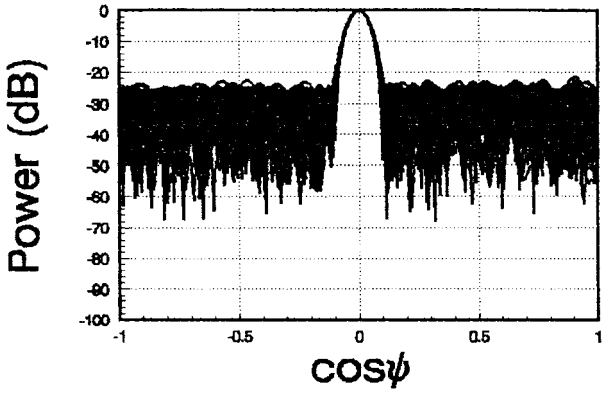

(a)

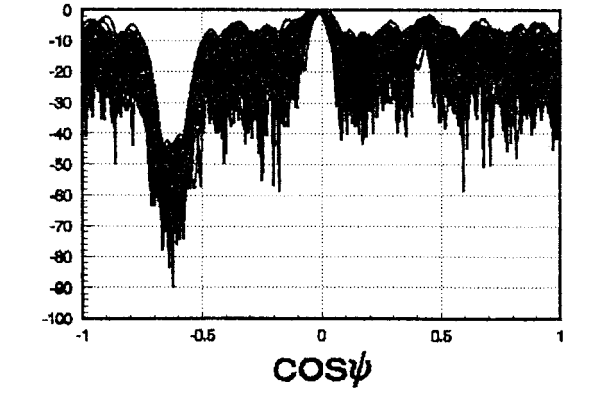

(b)

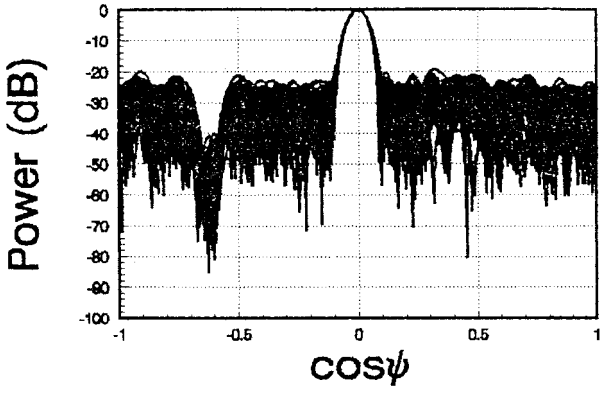

(c)

Fig. 2. Comparison of the quiescent patterns and the adapted patterns before and after using the new method in the presence of array, channel, and covariance matrix estimation errors. $E = 5\%$, $C = 10\%$, and $\mathrm{PSLD} = -20$ dB. (a) The quiescent patterns. (b) The adaptive patterns before using the new method. (c) The adaptive patterns after using the new method.

bin under test. In addition, the adaptive pattern has preserved very well the low sidelobe feature of the designed quiescent pattern (−40-dB peak sidelobes). However, array errors result in severe pattern distortion, as can be seen from Fig. 1(c). By comparing Fig. 1(b) and (c) it can be noted that even small array errors ($E = 5\%$) result in the rise of the peak sidelobe level of the adaptive pattern from −40 dB to −6 dB.

Now we use one example to demonstrate the performance of the proposed adaptive pattern control method. Assume that the array error standard deviation $E = 5\%$ and the channel error standard deviation $C = 10\%$ and $2N$ secondary data samples are used to estimate the clutter covariance matrix. One hundred independent trials are carried out and the random error and noise samples are changed from trial to trial. The results are shown in Fig. 2. Fig. 2(a) shows all the patterns in the 100 trials obtained by using the quiescent weights. Although the designed peak sidelobe level is −40 dB, the practical peak sidelobes rise up to −22 dB, which is exactly the corresponding PPSL predicted by (4). The adaptive patterns before and after using the new method are plotted in Fig. 2 (b) and (c), respectively, where the desired peak sidelobe level

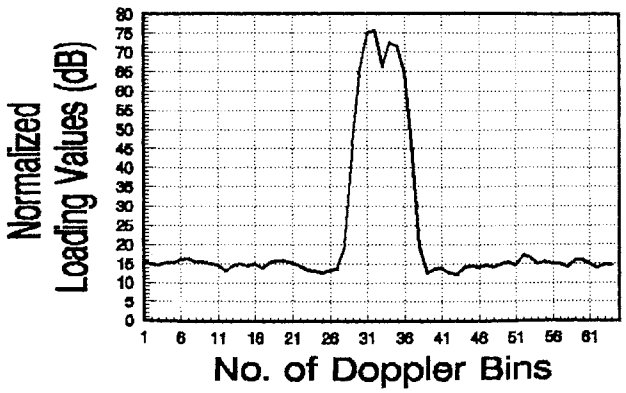

Fig. 3. Normalized loading values for all Doppler bins. $E = 5\%$, $C = 10\%$, and $\mathrm{PSLD} = -20$ dB.

(PSLD) is −20 dB. Note that although the margin between the PSLD and upper limit (PPSL) is only 2 dB, the new method can still precisely control the peak sidelobes of the adaptive patterns to the desired level. The normalized load values for all Doppler bins are plotted together in Fig. 3. Note that except for a few bins in the vicinity of the mainlobe clutter region (around No. 33 Doppler bin), the normalized loading values are almost the same (15 dB) for all Doppler bins. Hence, only one loading value needs to be computed online and the computational load can be shared by K Doppler bins. The loading values corresponding to those bins in the mainlobe clutter region tend to be very large and there are two reasons to it: one is because the dimensional size of the clutter subspaces in these bins is much larger than that in other Doppler bins and the other is because the pattern distortion is also caused by near mainlobe interference. In this case, we must make a good tradeoff between the pattern control quality and the clutter suppression performance. Applying a constant normalized loading value to all Doppler bins seems to be a good compromise.

V. Conclusion

In this paper, we have studied the effects of different errors on the array pattern distortion in space–time adaptive processing for airborne radar. A method is proposed to remedy the pattern distortion and it can precisely control the peak sidelobes of adapted patterns to the desired level. Although the method is presented for STAP, it can be applied directly to the conventional adaptive beamforming for rectangular planar arrays used to suppress jammers.

Appendix A
Derivation of (4)

By substituting $\mathbf{W}_k = \mathbf{S}_q$ into (1), we can obtain the quiescent pattern in the presence of array and channel errors, which has the following form:

$$H_q(u,v) = \sum_{n=1}^{N} A_n\left(1+\delta_n^c\right)\exp\left(j\phi_n^c\right)\sum_{m=1}^{M} I_m\left(1+\delta_{mn}^a\right) \times \exp\left(j\phi_{mn}^a\right)\exp[j(mu+nv)] \quad (12)$$

where $u = \frac{2\pi d_y}{\lambda}(\sin\varphi - \sin\varphi_0)$ and $v = \frac{2\pi d_x}{\lambda}(\cos\psi - \cos\psi_0)$. Without loss of generality, assume that $\sum_{n=1}^{N} A_n = 1.0$ and $\sum_{m=1}^{M} I_m = 1.0$. For small amplitude (δ) and phase (ϕ) errors, it follows:

$$(1+\delta)\exp(j\phi) \approx (1+\delta)(1+j\phi) \approx 1+\delta+j\phi. \quad (13)$$

Hence, $H_q(u,v)$ can be rewritten as

$$H_q(u,v) = \sum_{n=1}^{N} A_n\left(1+\delta_n^c+j\phi_n^c\right)\sum_{m=1}^{M} I_m\left(1+\delta_{mn}^a+j\phi_{mn}^a\right) \times \exp[j(mu+nv)] \quad (14)$$

$$\triangleq x + jy. \quad (15)$$

When the number of array elements is large, $H_q(u,v)$ is the sum of many independent random variables. According to Lindenberg and Levy's central limit theorem, under certain general conditions, the distribution of $H_q(u,v)$ approaches a normal distribution. The mean of $H_q(u,v)$ is given by

$$E[H_q(u,v)] = \sum_{n=1}^{N}\sum_{m=1}^{M} A_n I_m \exp[j(mu+nv)] \quad (16)$$

$$\triangleq \bar{x} + j\bar{y} \quad (17)$$

where $E(\cdot)$ denotes the expectation.

We now derive the variance of $H_q(u,v)$. Let $\sigma_x^2 \triangleq E[(x-\bar{x})^2]$, $\sigma_y^2 \triangleq E[(y-\bar{y})^2]$, and $\sigma_{xy} \triangleq E[(x-\bar{x})(y-\bar{y})]$. Then we have

$$E[|H_q(u,v) - E[H_q(u,v)]|^2] = E[|H_q(u,v)|^2] - |E[H_q(u,v)]|^2 \quad (18)$$

$$= \sigma_x^2 + \sigma_y^2 \quad (19)$$

and

$$E\{[H_q(u,v) - E[H_q(u,v)]]^2\} = E\{[H_q(u,v)]^2\} - \{E[H_q(u,v)]\}^2 \quad (20)$$

$$= \sigma_x^2 - \sigma_y^2 + 2j\sigma_{xy}. \quad (21)$$

By ignoring all the moments above the second order we have

$$\sigma_x^2 + \sigma_y^2 = \sum_{n=1}^{N}\sum_{m=1}^{M} A_n^2 I_m^2\left[\left(\sigma_a^a\right)^2 + \left(\sigma_\phi^a\right)^2\right] + \sum_{n=1}^{N} A_n^2\left[\left(\sigma_a^c\right)^2 + \left(\sigma_\phi^c\right)^2\right]|H_{\mathrm{sb}}(u)|^2 \quad (22)$$

and

$$\sigma_x^2 - \sigma_y^2 + 2j\sigma_{xy} = \sum_{n=1}^{N}\sum_{m=1}^{M} A_n^2 I_m^2\left[\left(\sigma_a^a\right)^2 - \left(\sigma_\phi^a\right)^2\right]\exp[2j(mu+nv)] + \sum_{n=1}^{N} A_n^2\left[\left(\sigma_a^c\right)^2 - \left(\sigma_\phi^c\right)^2\right]\exp(j2nv)[H_{\mathrm{sb}}(u)]^2 \quad (23)$$

where $H_{\mathrm{sb}}(u) = \sum_{m=1}^{M} I_m \exp(jmu)$. From (23), it can be noted that $\sigma_x^2 - \sigma_y^2 + 2j\sigma_{xy}$ is the sum of many exponential functions and $(\sigma_a^a)^2 - (\sigma_\phi^a)^2$ and $(\sigma_a^c)^2 - (\sigma_\phi^c)^2$tend to be small,

by the same argument as used in [13], it can be deduced that $\sigma_x^2 - \sigma_y^2 + 2j\sigma_{xy} \approx 0$ when compared to $\sigma_x^2 + \sigma_y^2$. Thus, in the principal plane corresponding to $u = 0$, both σ_x^2 and σ_y^2 reach the maximum values and

$$\sigma_x^2 \approx \sigma_y^2 \approx \frac{1}{2}\sum_{n=1}^{N} A_n^2\{(\sigma_a^c)^2 + (\sigma_\phi^c)^2 + \eta[(\sigma_a^a)^2 + (\sigma_\phi^a)^2]\} \tag{24}$$

$$= \frac{1}{2}\|\mathbf{S}_q\|_2^2\{(\sigma_a^c)^2 + (\sigma_\phi^c)^2 + \eta[(\sigma_a^a)^2 + (\sigma_\phi^a)^2]\} \tag{25}$$

where $\eta = \sum_{m=1}^{M} I_m^2$.

In [13], it was shown that the sidelobe level of the normalized radiation pattern obeys Rician distribution and general-purpose design curves were also given, which relate the peak sidelobe level to the above variances. Using (25) and these design curves, (4) is obtained.

It must be pointed out that the similar result of (25) in [13] was given as follows:

$$\sigma_x^2 \approx \sigma_y^2 \approx \frac{1}{2}\|\mathbf{S}_q\|_2^2\{(\sigma_a^c)^2 + (\sigma_\phi^c)^2 + \eta[(\sigma_a^c)^2 + (\sigma_\phi^c)^2 + (\sigma_a^a)^2 + (\sigma_\phi^a)^2]\}. \tag{26}$$

This result is incorrect. One simple way to verify it is to consider the special case when $M = 1$. In this case, the planar array degenerates to a linear array and $\eta = 1$. After some simple mathematical manipulations we have

$$\sigma_x^2 \approx \sigma_y^2 \approx \frac{1}{2}\|\mathbf{S}_q\|_2^2[(\sigma_a^c)^2 + (\sigma_\phi^c)^2 + (\sigma_a^a)^2 + (\sigma_\phi^a)^2]. \tag{27}$$

(27) is contradictory to the result given in (26).

Appendix B
Derivation of (11)

In addition to the uncontrollable pattern distortion caused by the real channel errors and the equivalent part of the array errors, in adaptive arrays, the perturbation of adaptive weights to the quiescent weight settings also results in pattern distortion. The difference between the adaptive and quiescent weights can be viewed as additional channel errors. Define the adaptive weight vectors equivalently as

$$\mathbf{W}_k = (\mathbf{I} + \tilde{\mathbf{C}}_a)\mathbf{S}_q \tag{28}$$

where $\tilde{\mathbf{C}}_a \triangleq \mathrm{diag}\{\tilde{\delta}_1^c + j\tilde{\phi}_1^c,\ \tilde{\delta}_2^c + j\tilde{\phi}_2^c, \ldots, \tilde{\delta}_N^c + j\tilde{\phi}_N^c\}$ with $\tilde{\delta}_n^c$ and $\tilde{\phi}_n^c$ $(1 \le n \le N)$ denoting the equivalent amplitude and phase errors in the nth channel due to the perturbation of adaptive weights to the quiescent weight settings.

Substituting (28) into (1) we obtain the corresponding adaptive pattern, which has the form

$$H_k(u,v) = \sum_{n=1}^{N} A_n(1 + \delta_n^c + j\phi_n^c)(1 + \tilde{\delta}_n^c + j\tilde{\phi}_n^c) \times \sum_{m=1}^{M} I_m(1 + \delta_{mn}^a + j\phi_{mn}^a)\exp[j(mu + nv)]. \tag{29}$$

Because the additional channel errors satisfy (8), it follows:

$$E[\|\mathbf{W}_k - \mathbf{S}_q\|_2^2] = \|\mathbf{W}_k - \mathbf{S}_q\|_2^2 = \epsilon_0^2\|\mathbf{S}_q\|_2^2. \tag{30}$$

The additional channel errors are approximately uncorrelated with the real array and channel errors. When they are independent random variables with zero means, it can be derived in the same way as used in Appendix A that

$$\sigma_x^2 \approx \sigma_y^2 \approx \frac{1}{2}\|\mathbf{S}_q\|_2^2\{\epsilon_0^2 + (\sigma_a^c)^2 + (\sigma_\phi^c)^2 + \eta[(\sigma_a^a)^2 + (\sigma_\phi^a)^2]\}. \tag{31}$$

Using (31) and the pattern design curves given in [13], (11) is obtained.

As pointed out in [11], generally speaking, the additional channel errors due to adaptive processing are correlated random variables with nonzero means because they must satisfy the constraint equation (8). However, (31) seems to be an approachable upper bound. Large simulation results confirm this conclusion and more theoretical analysis is given in [11] for adaptive beamforming based on uniform linear arrays in the presence of array and estimation errors.

References

[1] L. E. Brenann and I. S. Reed, "Theory of adaptive radar," *IEEE Trans. Aerosp. Electron. Syst.*, vol. AES-9, pp. 237–252, Mar. 1973.

[2] L. E. Brenann, D. J. Piwinski, and F. Staudaher, "Comparison of space-time adaptive processing approaches using experimental airborne data," in *Rec. IEEE Nat. Radar Conf.*, Boston, MA, Apr. 1993, pp. 176–181.

[3] R. Klemm, "Adaptive airborne MTI: An auxiliary approach," *Proc. Inst. Elect. Eng.*, vol. 134, pt. F, no. 3, pp. 269–276, June 1987.

[4] H. Wang and L. Cai, "On adaptive spatial-temporal processing for airborne surveillance radar system," in *Proc. Chinese Inst. Electron. Int. Conf. Radar*, Beijing, China, Oct. 1991, pp. 365–368.

[5] Z. Bao, G. Liao, R. Wu, Y. Zhang, and Y. Wang, "Adaptive spatial-temporal processing for airborne radar," *Chinese J. Electron.*, vol. 2, no. 1, pp. 1–7, Apr. 1994 (in English).

[6] H. Wang, H. R. Park, and M. C. Wicks, "Recent results in space-time adaptive processing," in *Rec. IEEE Nat. Radar Conf.*, Atlanta, GA, Mar. 1994, pp. 104–109.

[7] R. Wu and Z. Bao, "Training method in space-time adaptive processing with strong generalizing ability," in *Rec. IEEE Int. Radar Conf.*, Washington, DC, May 1995, pp. 603–608.

[8] W. F. Gabriel, "Using spectral estimation techniques in adaptive processing antenna systems," *IEEE Trans. Antennas Propogat.*, vol. AP-34, pp. 291–300, Mar. 1986.

[9] B. D. Carlson, "Covariance matrix estimation errors and diagonal loading in adaptive arrays," *IEEE Trans. Aerosp. Electron. Syst.*, vol. 24, pp. 397–401, July 1988.

[10] K. Gerlach, "Adaptive array transient sidelobe levels and remedies," *IEEE Trans. Aerosp. Electron. Syst.*, vol. 26, pp. 560–568, May 1990.

[11] R. Wu, Z. Bao, and Y. Ma, "Control of peak sidelobe level in adaptive arrays," *IEEE Trans. Antennas Propogat.*, vol. 44, pp. 1341–1347, Oct. 1996.

[12] R. Wu, *Space–Time Adaptive Processing for Airborne Phased Array Radar: Theory and Implementation*, Ph.D. dissertation, Xidian University, Xi'an, China, Dec. 1993.

[13] J. K. Hsiao, "Normalized relationship among errors and the sidelobe level," *Radio Sci.*, vol. 19, no. 1, pp. 292–302, Jan./Feb. 1984.

[14] K. Teitelbaum, "A flexible processor for a digital adaptive array radar," *IEEE Aerosp. Electron. Syst. Mag.*, vol. 6, pp. 18–22, May 1991.

Renbiao Wu (M'95) was born in February 1967 in Wuhan, China. He received the B.Sc. and M.Sc. degrees from Northwestern Polytechnic University, Xi'an, China, in 1988 and 1991, respectively, and the Ph.D. degree from Xidian University, Xi'an, China, in 1994, all in electrical engineering.

From May 1994 to February 1996, under a grant from China Postdoc Council, he was a Postdoctoral Fellow at the College of Marine Engineering, Northwestern Polytechnic University, China, where he was promoted to Associate Professor in December 1995. From March 1996 to February 1997, he was a Postdoctoral Associate at the Center for Transportation Research, Virginia Polytechnic Institute and State University (Virginia Tech). Since March 1997, he has been a Postdoctoral Associate at the Department of Electrical and Computer Engineering, University of Florida. His current research interests include spectral estimation, feature extraction, and image formation for synthetic aperture radar, space–time adaptive processing for airborne radar, adaptive arrays, and high-resolution array signal processing.

Dr. Wu is a Senior Member of the Chinese Institute of Electronics.

Zheng Bao (SM'85) was born in 1927 in Nantong, China. He received the B.Sc. degree from the Communication Engineering Institute of China, Hebei, China, in 1953.

He is currently a Professor and Chairman for the Academic Council at the State Key Laboratory for Radar Signal Processing, Xidian University, Xi'an, China. He has authored or coauthored six books and more than 200 papers. His research fields include radar system, signal processing, and circuit theory.

Mr. Bao is a Member of the Chinese Academy of Sciences.